Observations of Time-dependent Errors in Long-period Instrument Gain at Global Seismic Stations

Göran Ekström, Colleen A. Dalton, and Meredith Nettles
Department of Earth and Planetary Sciences, Harvard University, Cambridge, MA

SUMMARY

We present evidence for significant deviations of the true instrument gain from that reported for several modern broad-band permanent seismograph stations. Our result derives from a systematic comparison of observed and synthetic long-period seismograms for approximately 600 large earthquakes. Seismograms were collected from globally distributed stations and analyzed using the centroid-moment-tensor (CMT) algorithm for estimating earthquake parameters. Following the source inversion, synthetic seismograms corresponding to the final earthquake parameters were compared with the observed seismograms and an optimal amplitude-scaling coefficient for each seismogram was determined. Scaling coefficients for earthquakes occurring in a given calendar year were then averaged to investigate the temporal stability of instrument gain. Data for up to 15 years (1990–2004) for more than 200 stations were processed. Most stations show good agreement (±10%) between the observed and reported gains. A small number of stations display a larger constant offset in the gain, probably caused by errors in the reported absolute gain or, potentially, by unmodeled systematic effects resulting from the Earth's lateral heterogeneity. The existence of errors in the reported long-period gain is confirmed through a station-by-station comparison with results from an independent analysis of station-gain bias at similar periods. More than 15 stations display significant reductions in the true long-period gain that occur gradually over several months to a few years. At ~250-s period, these changes are as large as 50% of the reported gain. The changes are smaller at shorter periods, suggesting a frequency-dependent modification of the instrument response. All of the affected stations showing a time-dependent deterioration are equipped with the Streckeisen STS-1 seismometer, suggesting a common cause for the observed behavior.

INTRODUCTION

Modern broad-band observatory seismometers are generally believed to have very stable instrument parameters. Earlier seismological instruments were less stable, with mechanical and electronic systems that tended to drift over time, leading to significant variations in the instrument response functions. Such temporal variations motivated the implementation of regular calibration of the seismographic systems, usually by means of step or sine-wave calibrations. The practice of recording daily step calibrations, employed in the 1960s for the analog World Wide Standardized Seismograph Network (WWSSN), was continued in the 1970s in the operation of the first digital global network, the High-Gain Long-Period (HGLP) network. The systematic recording of calibration pulses at the HGLP stations made it possible for Ekström and Nettles (1997) to determine accurate instrument response functions for these stations and to use the 20-year-old data in quantitative waveform-matching analyses of major earthquakes.

In the 1980's, daily sine-wave calibrations were also routine in the operation of most stations of the Global Digital Seismographic Network (GDSN), the predecessor of the current Global Seismographic Network (GSN). While Woodward and Masters (1989) demonstrated that the GDSN calibration pulses could be used to obtain detailed information about temporal variations of the instrument characteristics, many researchers viewed the daily calibrations, which removed at least 10 minutes of available data from each 24-hour time window, as unnecessary and detrimental to the scientific use of the network.

Starting in 1986, with the deployment of force-feedback very-broad-band seismometers (Wielandt and Steim, 1986) in the GSN, the practice of regular and frequent calibration was abandoned. The stability of the new sensors (Streckeisen STS-1 and Geotech KS-54000) and electronics, as well as the desire to have very long (days) uninterrupted time series motivated this decision. Calibrations of the instruments are now generally performed only during maintenance visits to the stations. In practice, this means that for some stations the interval between calibrations is one or more years.

While the assertion of response stability for modern systems seems, in general, to be consistent with the performance of the instruments, our research group has on several occasions noticed significant disagreement between the amplitudes of observed and predicted waveforms at certain stations. These observations have resulted mainly from our routine analysis of earthquakes as part of the Harvard CMT Project (Dziewonski *et al.*, 1981; Ekström *et al.*, 2005). It is, however, difficult to arrive at firm conclusions concerning the cause of the mismatch based on only a small number of observations. Many factors other than instrument errors, including unmodeled aspects of three-dimensional Earth structure and earthquake complexity, cause differences between observed and synthetic waveforms. We have also observed the need for gain correction factors in tomographic inversions for surface-wave phase velocities and attenuation (Dalton and Ekström, 2004, 2005). The lack of recorded calibration signals makes it difficult to validate the anomalous observations, and other methods must be used.

In this paper, we present the results of an experiment aimed at identifying stations with response-function problems using systematic differences between observed and synthetic seismograms. One important result from the analysis presented here is that most stations we have investigated have responses that agree well with those reported. For a small subset of stations, however, gradual but clear changes are seen in the ratio of observed to synthetic amplitudes. The main purpose of this paper is to document the existence and gross character of this problem. We do not offer an explanation, but hope that this work will serve as motivation for a detailed technical investigation and the development of a remedy.

METHOD

We selected all earthquakes of $M_W > 6.5$ occurring between 1990 and 2004 for our analysis. Events of this size are well recorded by the global networks in the period range used in the CMT analysis (50–400 s). Approximately 40 earthquakes of this size occur each year. The data were collected from a variety of networks: the IRIS-USGS Global Seismographic Network (GSN, network codes II and IU) (Butler *et al.*, 2004), Geoscope (G), GEOFON (GE), Mednet (MN), the Canadian Seismograph Network (CN), the Berkeley Digital Seismograph Network (BK), the China Digital Seismograph Network (CDSN, network codes CD and IC), the Global Telemetered Seismic Network (GTSN, network code GT), and a few additional stations. Seismograms from the long-period (LH) and very-long-period (VH) channels from the primary sensor were used in the analysis. For those stations equipped with additional sensors, usually a Streckeisen STS-2 or Güralp CMG-3T seismometer, the data from the second sensor were not used as constraints in the CMT inversion, but amplitude-scaling factors were calculated. Those stations for which only broad-band data (BH) are available, such as the GTSN stations in their current configuration, were not included. For practical reasons, we did not include data for all years for all networks. The data from the GSN, Geoscope, Mednet, and CDSN networks are nearly complete for the 15-year time period.

The data were assembled and filtered as in our standard CMT analysis (Ekström *et al.*, 2005). An essential detail in the processing is a correction for the reported instrument response function. For all of the data, we used the best currently available instrument responses in the analysis. These responses were obtained in the form of "dataless SEED" volumes from the IRIS Data Management Center or from the network operators. The instrument parameters we used were updated in June, 2005.

The CMT analysis involves matching long-period three-component seismograms in an inversion that results in estimates of the earthquake moment tensor and its centroid in space and time. For the earthquakes considered here, three types of waveforms are used in the CMT analysis: (1) body waves, which are here defined as the intermediate-period (50–150 s) waveforms that arrive before the fundamental-mode surface waves; (2) mantle waves, which are the long-period (200–400 s) waveforms recorded during the first few hours after the earthquake and dominated by long-period multiple-orbit Love and Rayleigh waves; and (3) surface waves, which are the intermediate-period (50–150 s) minor-arc surface-wave arrivals.

To process the large number of seismograms considered without extensive involvement by an analyst, we rely on an automated algorithm to select and edit the data used in the source inversion. In the initial inversion, the automatic editor selects data based on criteria related directly to the character of the long-period signal. For example, signal-to-noise ratios within a trace are calculated in a series of time windows and compared with the signal level expected given the distance to the event. After seismogram selection, an initial CMT is calculated with the centroid location fixed.

Following the initial inversion, the automatic editor compares all of the waveforms, including those that were initially deselected, with the synthetic waveforms generated from the moment tensor resulting from the first step. Based on fit and correlation, the editor makes new choices, and the inversion is repeated. In the second and subsequent steps, the depth and epicenter of the earthquake are allowed to change. The better centroid obtained and the better-informed selection of waveforms usually lead to a much improved fit to the waveforms. The objective of the automatic editor, however, is not to minimize the residual variance, but rather to maximize the inclusion of data where signal is definitely present.

For earthquakes of the size considered here ($M_W > 6.5$), the data from the global networks are generally very good, and seismograms from most stations are included in the analysis. Some stations, mainly those located on small ocean islands, can have very high levels of long-period noise on the horizontal components, and these components may therefore not be selected to contribute to the CMT solution. Because of the great number of stations contributing to the final earthquake result (more than 100 for a majority of the earthquakes discussed here), the CMT results are very robust. The moment tensors obtained in the automatic analysis agree well with results in the analyst-reviewed CMT catalog (Dziewonski *et al.*, 1981; Ekström *et al.*, 2005).

In the final step of the CMT analysis, synthetic seismograms are calculated for all stations and components. Figure 1 (top panel) shows examples of the fit to body waves at station CCM (Cathedral Caves, Missouri) for an earthquake on June 10, 2004. The agreement between observed and synthetic waveforms is generally very good. Figure 1 (bottom panel) shows examples of the fit to mantle waves at station NNA (Ñaña, Peru) for the same earthquake. We quantify the agreement between the predicted and observed waveforms using the residual normalized variance (misfit) and the correlation. The misfit F is calculated as

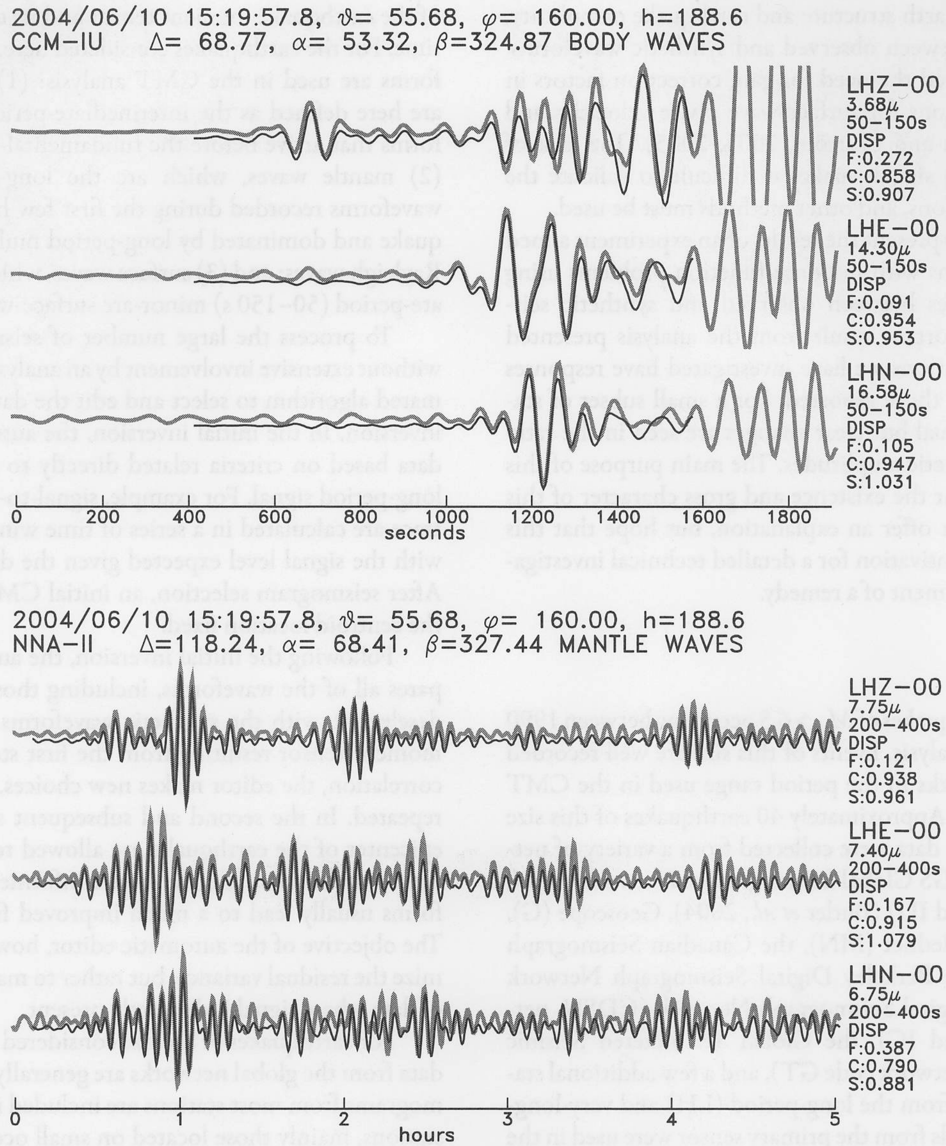

▲ **Figure 1** (top panel). Comparison of observed (gray trace) and synthetic (black trace) body waves for station CCM-IU for the June 10, 2004 M_W = 6.8 Kamchatka earthquake. The channel name, maximum displacement, and values for the three parameters F, C, and S are given to the right of each pair of waveforms. (bottom panel) Comparison of observed (gray trace) and synthetic (black trace) mantle waves for station NNA-II for the June 10, 2004 M_W = 6.8 Kamchatka earthquake.

$$F = \frac{\sum_{i=1}^{N}\left(o_i - s_i\right)^2}{\sum_{i=1}^{N} o_i^2} \qquad (1)$$

where o_i is the observed time series, N is the number of selected time points, and s_i is the synthetic time series. The correlation C is

$$C = \frac{\sum_{i=1}^{N} o_i s_i}{\sqrt{\left(\sum_{i=1}^{N} o_i^2\right)\left(\sum_{i=1}^{N} s_i^2\right)}} \qquad (2)$$

A third parameter considered is the scaling factor S, which is the factor by which the synthetic seismogram should be multiplied in order to achieve the smallest misfit,

$$S = \frac{\sum_{i=1}^{N} o_i s_i}{\sum_{i=1}^{N} s_i^2} \qquad (3)$$

A value of S smaller than 1.0 would thus be consistent with the true gain of the seismometer being smaller than the reported gain, and a value larger than 1.0 with the true gain being larger than the reported gain. Values of F, C, and S are given for each seismogram shown in Figure 1. The scaling factor S is the variable used here to examine systematic variations in observed and reported gain at different stations.

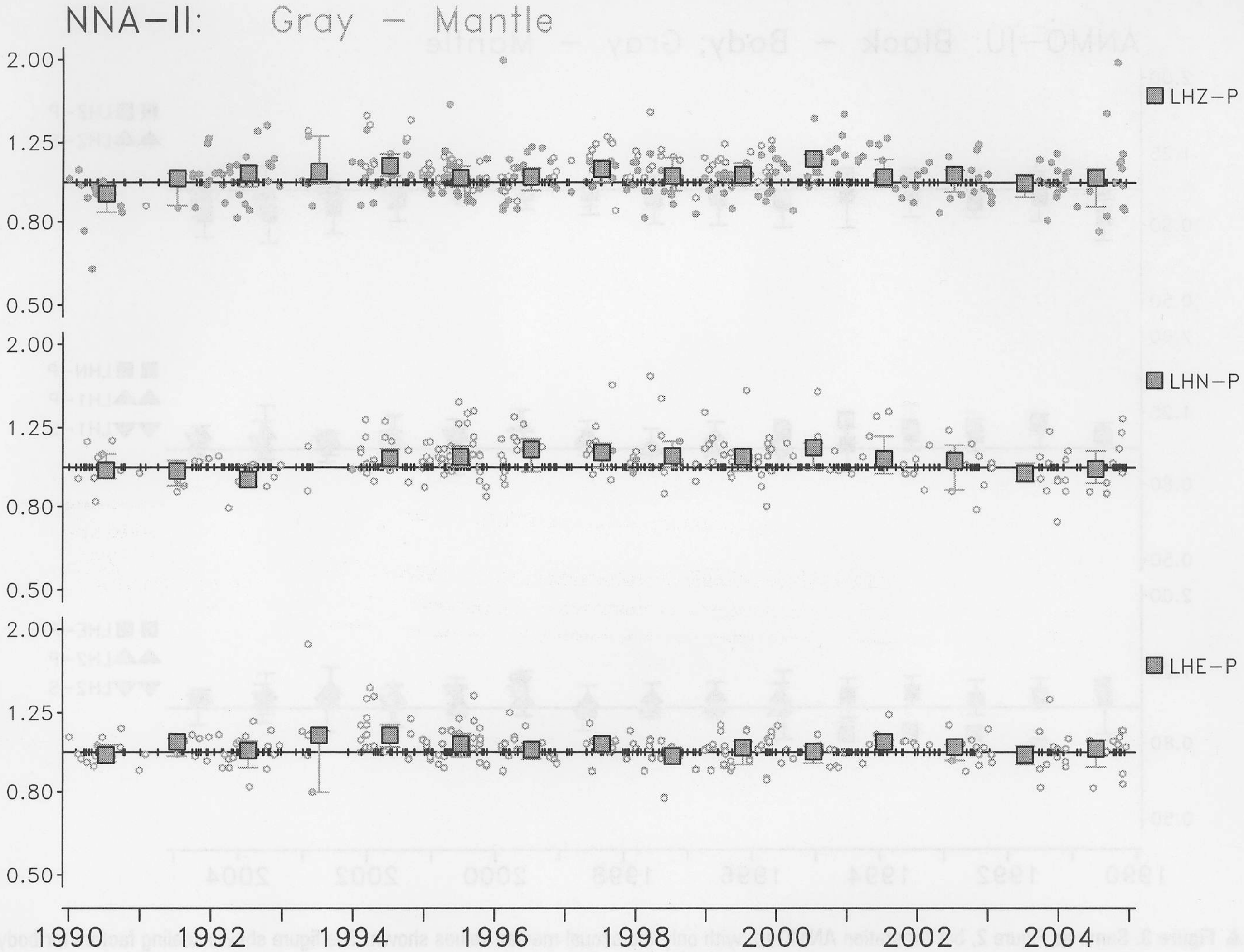

▲ **Figure 2.** Scaling factors for station NNA-II for the period 1990—2004. Small hexagons show scaling factors for individual traces. Large square symbols show the median scaling factor for each year, with the error bars corresponding to the range of the second and third quartiles of the scaling factors. The legend on the right identifies the symbol type with a specific channel, with -P referring to the primary sensor. There is no indication of a problem with this station.

RESULTS

In total, 626 earthquakes were analyzed for this study. We discarded 28 of the events owing to poor data quality or poor convergence in the inversion. The discarded events were mostly earthquakes that overlapped in time with other large earthquakes. The total number of stations was 330, though a small number of these were duplicates, as some stations contribute to more than one network and some stations have changed network affiliation during the 15 years covered by this study. Synthetic seismograms corresponding to 934,367 observed seismograms were calculated, leading to an equal number of derived scaling factors.

Scaling factors for each station and channel were displayed and interpreted for stability and potentially anomalous behavior. Figure 2 shows an example of the data available for the Ñaña, Peru station (NNA-II) for the period 1990–2004. The diagram shows the scaling factors for each of the three components for mantle-wave data, which have peak sensitivity between 200 and 250 s. The vertical scale is logarithmic and the small symbols show values for individual event-seismogram pairs.

The scatter in the raw data for NNA-II is small, with the vast majority of the scaling values falling within the range 0.80–1.25 for all three components. We believe this scatter is not caused by the station, but rather by unmodeled effects of lateral heterogeneity and possibly by inadequacies in the normal-mode calculation of the synthetic seismograms. Effects of surface-wave refraction, lateral variations in attenuation, and mode coupling are, for example, not included in the calculation. Some of these effects can be systematic, given the relatively constant geographical distribution of earthquakes, and we do not attempt here to provide an explanation for individual deviations or small average offsets of the scaling factors. Instead, we focus on temporal trends in the data.

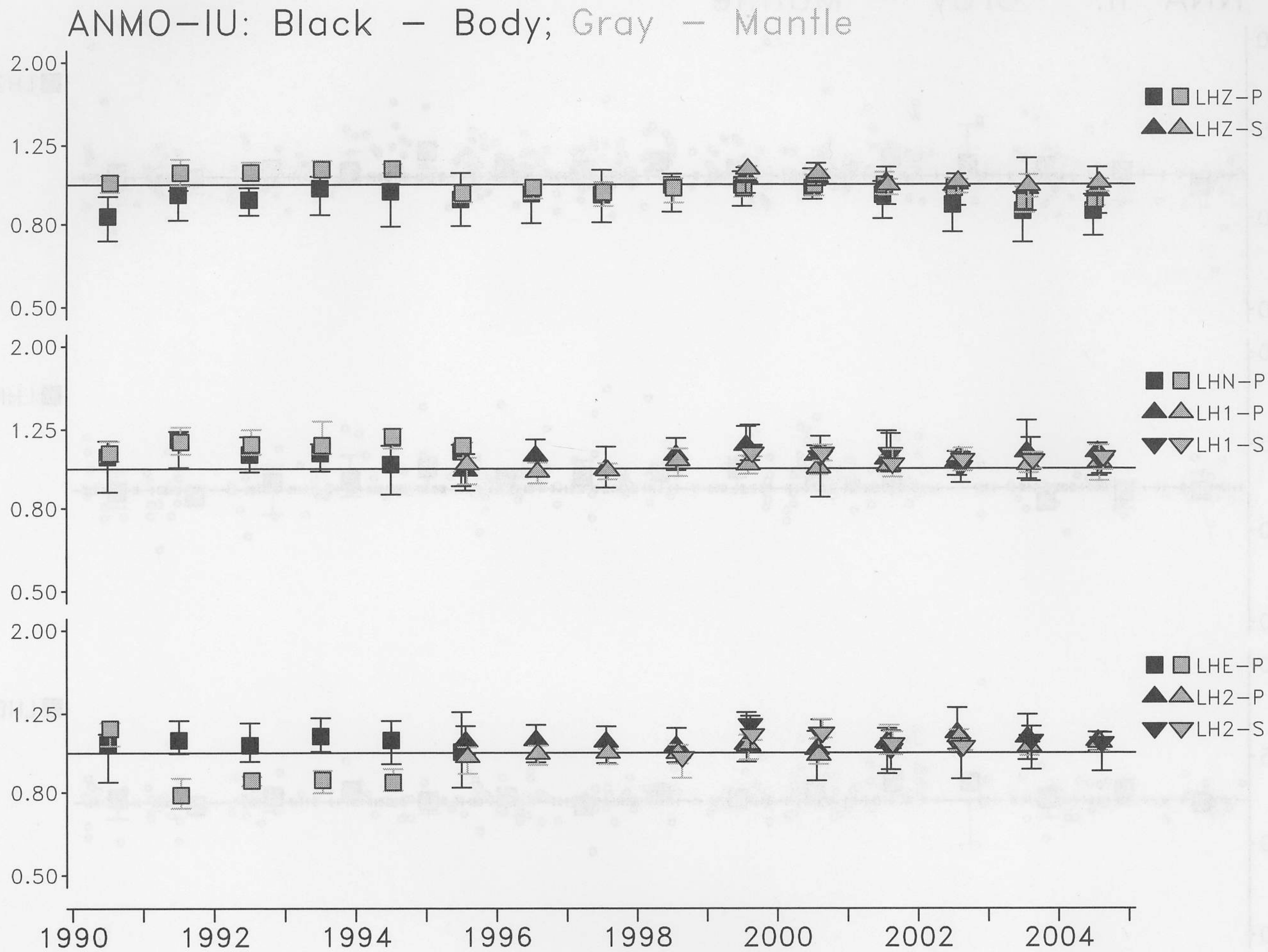

▲ **Figure 3.** Same as Figure 2, but for station ANMO-IU, with only the annual median values shown. The figure shows scaling factors for body waves (dominant period, 50–75 s) as well as for mantle waves. Channel names ending in -S refer to a secondary seismometer; the good agreement between the two seismometers on all components suggests that the reported gains do not deviate significantly from the true gains.

To examine potential temporal trends, we calculate an annual median value and an uncertainty defined by the range of the second and third quartiles of the scaling factors. As expected, the annual scaling factors show a much smaller scatter (Figure 2) than the individual measurements, and for station NNA-II we see no indication that the channel sensitivities have changed with time.

Figure 3 shows the annual values obtained for Albuquerque, New Mexico (ANMO-IU), the station for which we have the largest number of scaling values. The figure shows the scaling factors for both mantle waves and body waves, the latter having peak sensitivity between 50 and 75 seconds. There is one potentially significant change in the scaling factors that occurs in 1995, when the absolute scaling factors appear to change for both period bands. We believe this change coincides in time with the replacement of the KS-36000i seismometer at ANMO-IU by a KS-54000, as reported in the dataless SEED volume. The clear change in the relative scaling factors between the body- and mantle-wave bands that occurs at this time is indicative of a frequency-dependent problem with the response of either the former or the latter instrument. For the period 1998–2004, we obtain scaling factors for two instruments operating at the ANMO-IU site, identified as Primary (*P*) or Secondary (*S*) in Figure 3. The secondary sensor is a Güralp CMG-3T seismometer. The nearly identical scaling factors for the two instruments provide an indication that the reported gains during this time period are correct.

Figure 4 shows the annual values for San Pablo, Spain (PAB-IU). Here we see an example of a gradual change occurring on one of the components. The scaling factor for the East-West component begins to decline in 1999, and the scaling factor for mantle waves has by 2004 reached a value smaller than 0.5. It should be noted that the scaling factor for body waves also appears to decline, but not by the same amount, indicative of a frequency-dependent change in the instrument gain.

Figure 5 shows results for the station at Lovozero, Russia (LVZ-II). The trend for the vertical component is similar to that observed at PAB-IU. In 1996, the scaling factor begins to decline, and by 2000 it has reached 0.5 at mantle-wave periods.

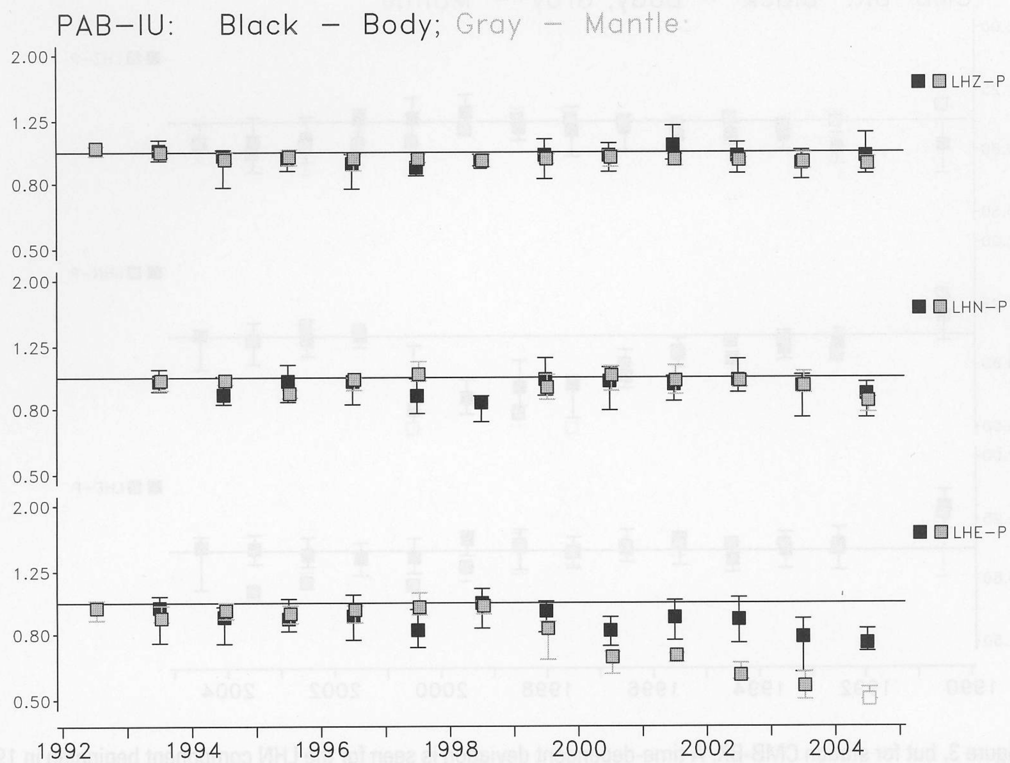

▲ **Figure 4.** Same as Figure 3, but for station PAB-IU. Beginning in 1999, the LHE-P component shows a time-dependent deviation of the observed gain from the reported gain. The deviation is larger for the longer-period (mantle-wave) data. The open square for year 2004 indicates that the scaling factor was smaller than 0.5.

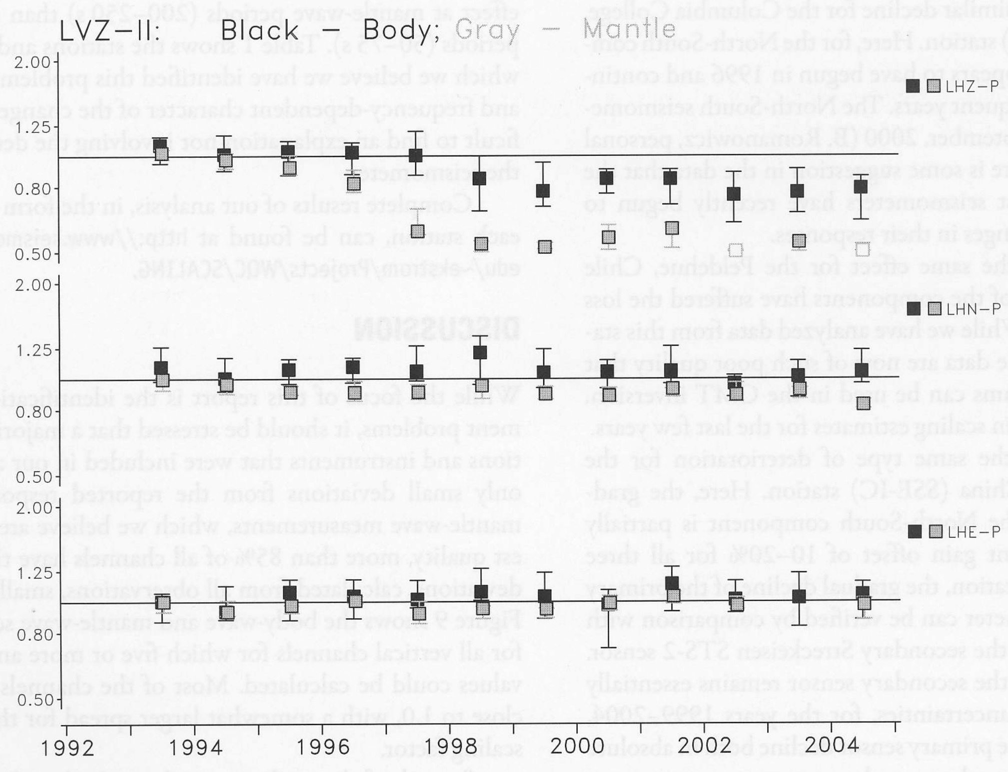

▲ **Figure 5.** Same as Figure 3, but for station LVZ-II. A time-dependent deviation is seen for the LHZ-P component beginning in 1996. Open symbols indicate scaling values smaller than 0.5.

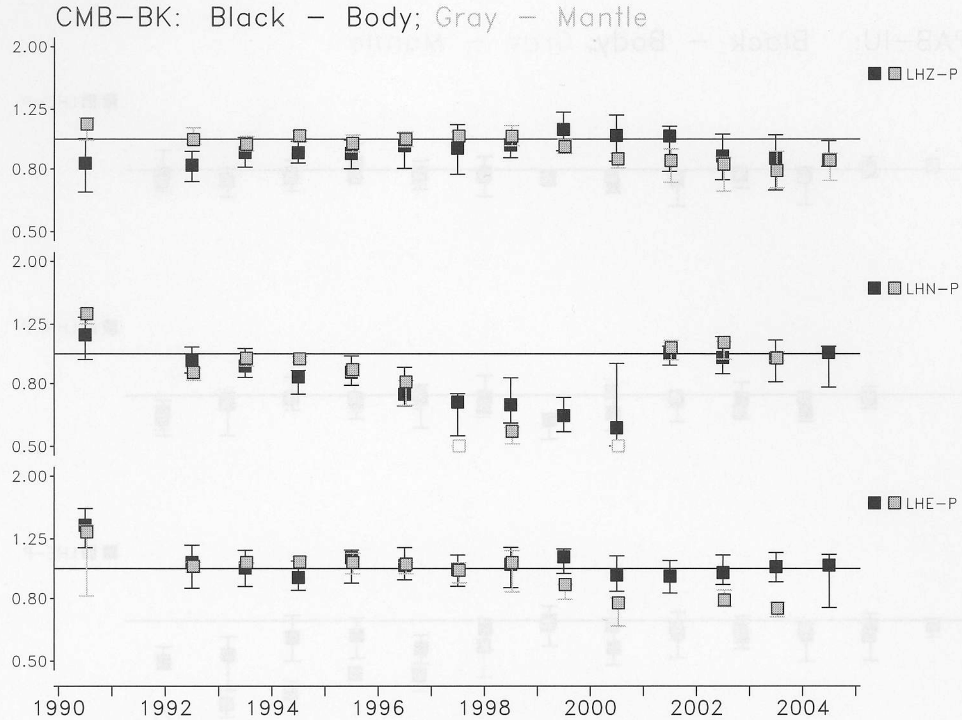

▲ **Figure 6.** Same as Figure 3, but for station CMB-BK. A time-dependent deviation is seen for the LHN component beginning in 1996 and ending in 2000. The North-South seismometer was replaced in September, 2000. There is a suggestion in the data that the LHE and LHZ components may have begun deteriorating in 1999. Open symbols indicate scaling values smaller than 0.5.

Again, the scaling factors at body-wave periods are less affected, indicative of a frequency-dependent change in gain.

Figure 6 shows a similar decline for the Columbia College, California (CMB-BK) station. Here, for the North-South component, the decline appears to have begun in 1996 and continued over several subsequent years. The North-South seismometer was replaced in September, 2000 (B. Romanowicz, personal communication). There is some suggestion in the data that the vertical and East-West seismometers have recently begun to experience similar changes in their responses.

Figure 7 shows the same effect for the Peldehue, Chile (PEL-G) station. All of the components have suffered the loss of long-period gain. While we have analyzed data from this station through 2004, the data are now of such poor quality that none of the seismograms can be used in the CMT inversion. We are unable to obtain scaling estimates for the last few years.

Figure 8 shows the same type of deterioration for the Sheshan, Shanghai, China (SSE-IC) station. Here, the gradual change seen on the North-South component is partially obscured by a constant gain offset of 10–20% for all three components. At this station, the gradual decline of the primary North-South seismometer can be verified by comparison with the scaling factors for the secondary Streckeisen STS-2 sensor. The scaling factor for the secondary sensor remains essentially constant, within the uncertainties, for the years 1999–2004, while the factors for the primary sensor decline both in absolute value and with respect to the secondary sensor.

The five examples shown here (PAB-IU, LVZ-II, CMB-BK, PEL-G, SSE-IC) illustrate a problem common to a number of stations we have examined. The main symptom that we observe is a gradual reduction in the scaling factor, with a larger effect at mantle-wave periods (200–250 s) than at body-wave periods (50–75 s). Table 1 shows the stations and channels for which we believe we have identified this problem. The gradual and frequency-dependent character of the change makes it difficult to find an explanation not involving the deterioration of the seismometer.

Complete results of our analysis, in the form of graphs for each station, can be found at http://www.seismology.harvard.edu/~ekstrom/Projects/WQC/SCALING.

DISCUSSION

While the focus of this report is the identification of instrument problems, it should be stressed that a majority of the stations and instruments that were included in our analysis show only small deviations from the reported response. For our mantle-wave measurements, which we believe are of the highest quality, more than 85% of all channels have time-averaged deviations, calculated from all observations, smaller than 15%. Figure 9 shows the body-wave and mantle-wave scaling factors for all vertical channels for which five or more annual median values could be calculated. Most of the channels have factors close to 1.0, with a somewhat larger spread for the body-wave scaling factor.

Several of the outliers are channels that display a time-dependent gain problem and are listed in Table 1. The remaining outliers display nearly constant offsets over time. While it

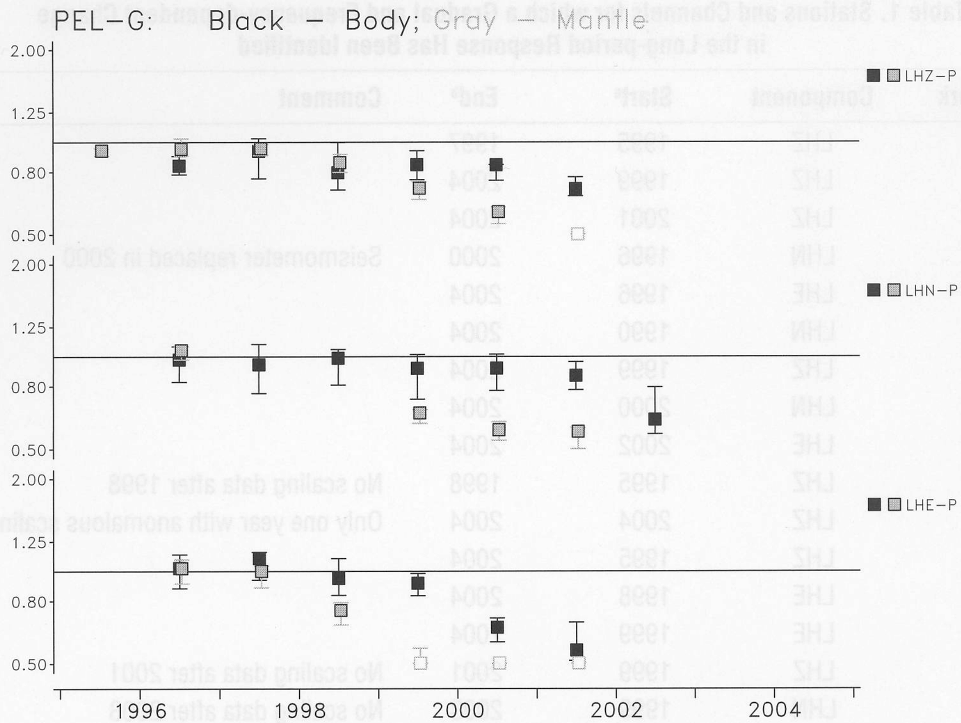

▲ **Figure 7.** Same as Figure 3, but for station PEL-G. Time-dependent deviations are seen on all components beginning in 1998 and 1999. Seismograms are available through 2004, but after 2001—2002 they are not of sufficient quality to obtain scaling factors. Open symbols indicate scaling values smaller than 0.5.

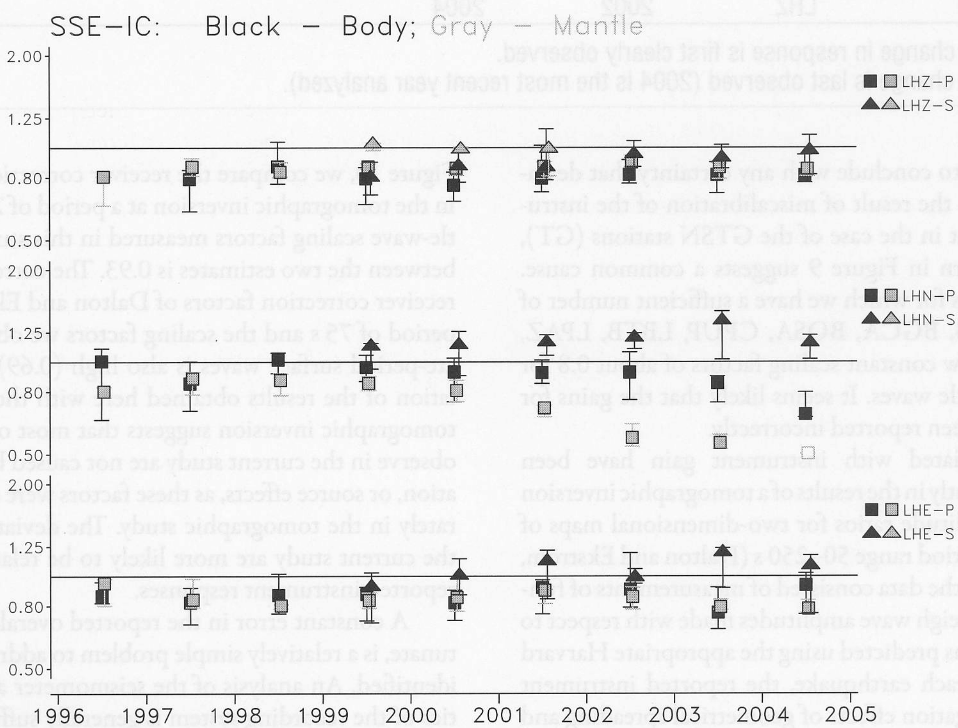

▲ **Figure 8.** Same as Figure 3, but for station SSE-IC. A time-dependent deviation is seen for the LHN-P component starting in 2000. The difference in scaling factors between the primary (-P) and secondary (-S) sensors is consistent with a decline in the true gain of the primary sensor. Open symbols indicate scaling values smaller than 0.5.

Table 1. Stations and Channels for which a Gradual and Frequency-dependent Change in the Long-period Response Has Been Identified

Station	Network	Component	Start[a]	End[b]	Comment
ABKT	II	LHZ	1995	1997	
BJT	IC	LHZ	1999	2004	
BRVK	II	LHZ	2001	2004	
CMB	BK	LHN	1996	2000	Seismometer replaced in 2000
HRV	IU	LHE	1996	2004	
HRV	IU	LHN	1990	2004	
KCC	BK	LHZ	1999	2004	
KCC	BK	LHN	2000	2004	
KCC	BK	LHE	2002	2004	
KEG	MN	LHZ	1995	1998	No scaling data after 1998
KIP	IU	LHZ	2004	2004	Only one year with anomalous scaling
LVZ	II	LHZ	1995	2004	
MA2	IU	LHE	1998	2004	
PAB	IU	LHE	1999	2004	
PEL	G	LHZ	1999	2001	No scaling data after 2001
PEL	G	LHN	1999	2003	No scaling data after 2003
PEL	G	LHE	1998	2001	No scaling data after 2001
PET	IU	LHN	2002	2004	
SAO	BK	LHZ	2001	2004	
SSE	IC	LHN	2000	2004	
SSB	G	LHZ	2002	2004	

a. Year in which the change in response is first clearly observed.
b. Year in which the change is last observed (2004 is the most recent year analyzed).

is generally difficult to conclude with any certainty that deviations of 10–20% are the result of miscalibration of the instrument, we believe that in the case of the GTSN stations (GT), the consistent pattern in Figure 9 suggests a common cause. All eight GT stations for which we have a sufficient number of observations (BDFB, BGCA, BOSA, CPUP, LBTB, LPAZ, PLCA, VNDA) show constant scaling factors of about 0.8 for both body and mantle waves. It seems likely that the gains for these stations have been reported incorrectly.

Problems associated with instrument gain have been observed independently in the results of a tomographic inversion of surface-wave amplitude ratios for two-dimensional maps of attenuation in the period range 50–250 s (Dalton and Ekström, 2005). In that study, the data consisted of measurements of fundamental-mode Rayleigh wave amplitudes made with respect to synthetic seismograms predicted using the appropriate Harvard CMT solution for each earthquake, the reported instrument response, and propagation effects of geometrical spreading and attenuation calculated for the Earth model PREM (Dziewonski and Anderson, 1981). At each period, four quantities were determined from the inversion: amplitude correction factors for each event, amplitude correction factors for each receiver, and spherical-harmonic maps of attenuation and phase velocity. In Figure 10, we compare the receiver correction factors obtained in the tomographic inversion at a period of 250 s with the mantle-wave scaling factors measured in this study. The correlation between the two estimates is 0.93. The correlation between the receiver correction factors of Dalton and Ekström (2005) for a period of 75 s and the scaling factors we obtain for intermediate-period surface waves is also high (0.69). The strong correlation of the results obtained here with those obtained in the tomographic inversion suggests that most of the deviations we observe in the current study are not caused by focusing, attenuation, or source effects, as these factors were accounted for separately in the tomographic study. The deviations we observe in the current study are more likely to be related to errors in the reported instrument responses.

A constant error in the reported overall gain, while unfortunate, is a relatively simple problem to address once it has been identified. An analysis of the seismometer and the characteristics of the recording system is generally sufficient to determine the correct gain. The most troubling problem identified in this study is the temporal variation of the true gain factor observed for many STS-1 seismometers. Based on our analysis, we infer that the gain factors are frequency dependent, and any retroactive corrections to the response information will be complex.

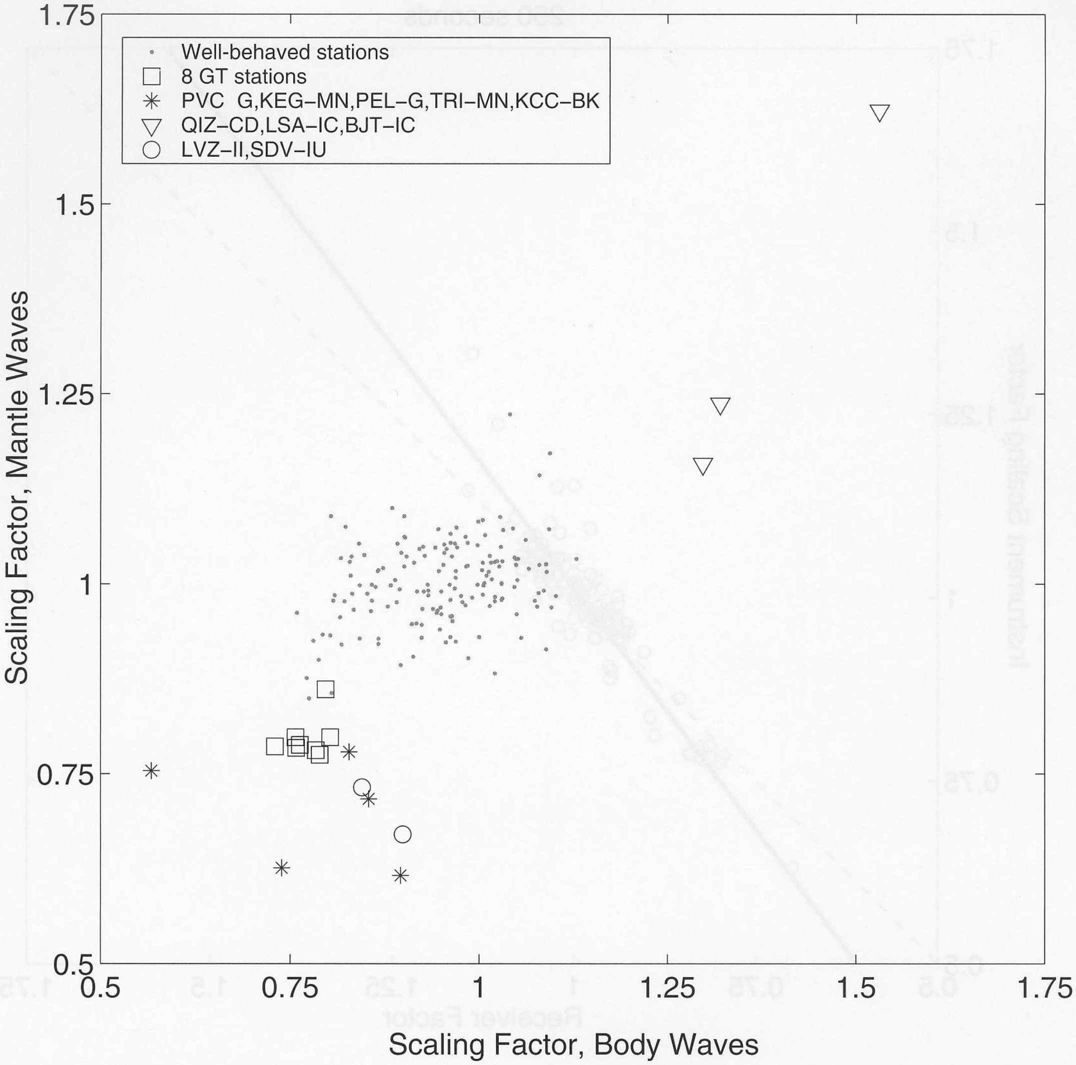

▲ **Figure 9.** Comparison of body-wave and mantle-wave scaling factors calculated for the 181 vertical-component channels for which we have at least five years of annual median values for both mantle waves and body waves. Small dots are used to represent stations for which the deviations are relatively small. Groups of stations displaying significant deviations are identified by specific symbols. Eight stations of the GTSN network deviate by approximately 20% from the expected value of 1.0.

Any repairs of the response information would be aided by a better understanding of the underlying cause of the problem. Plausible explanations for the observed decline in gain, such as the deterioration of electrical components in the system, are likely to cause changes in the phase response of the system as well. Approximately 15% of the stations equipped with STS-1 seismometers and for which we have sufficient data exhibit the behavior described here. The nature of the problem suggests that, over time, the problem may develop at additional stations.

In summary, we have identified several examples of probable instrument miscalibration and deterioration using an empirical approach in which recorded earthquake signals are employed as output calibration signals and synthetic seismograms as input calibration signals. This approach is not optimal and would not have been necessary if standard calibrations were routine in the operation of modern seismographic stations. The response problems we have identified with the STS-1 seismometer are serious, and raise the question of whether smaller deviations, on the order of 10%, are common. Errors of this size cannot be identified using the technique presented here, but are important for scientific research.

We recommend that regular calibrations, with published characteristics, be reintroduced into the operation of modern seismographic networks and that routine analysis of such calibrations be instituted.

ACKNOWLEDGMENTS

We thank Erhard Wielandt, Barbara Romanowicz, Bob Hutt, Pete Davis, and Kent Anderson for helpful discussions. Benedict Holland contributed in the early stages of the analysis. This work was funded by National Science Foundation Award EAR-0207608 and an IRIS subaward supporting the Harvard Waveform Quality Center.

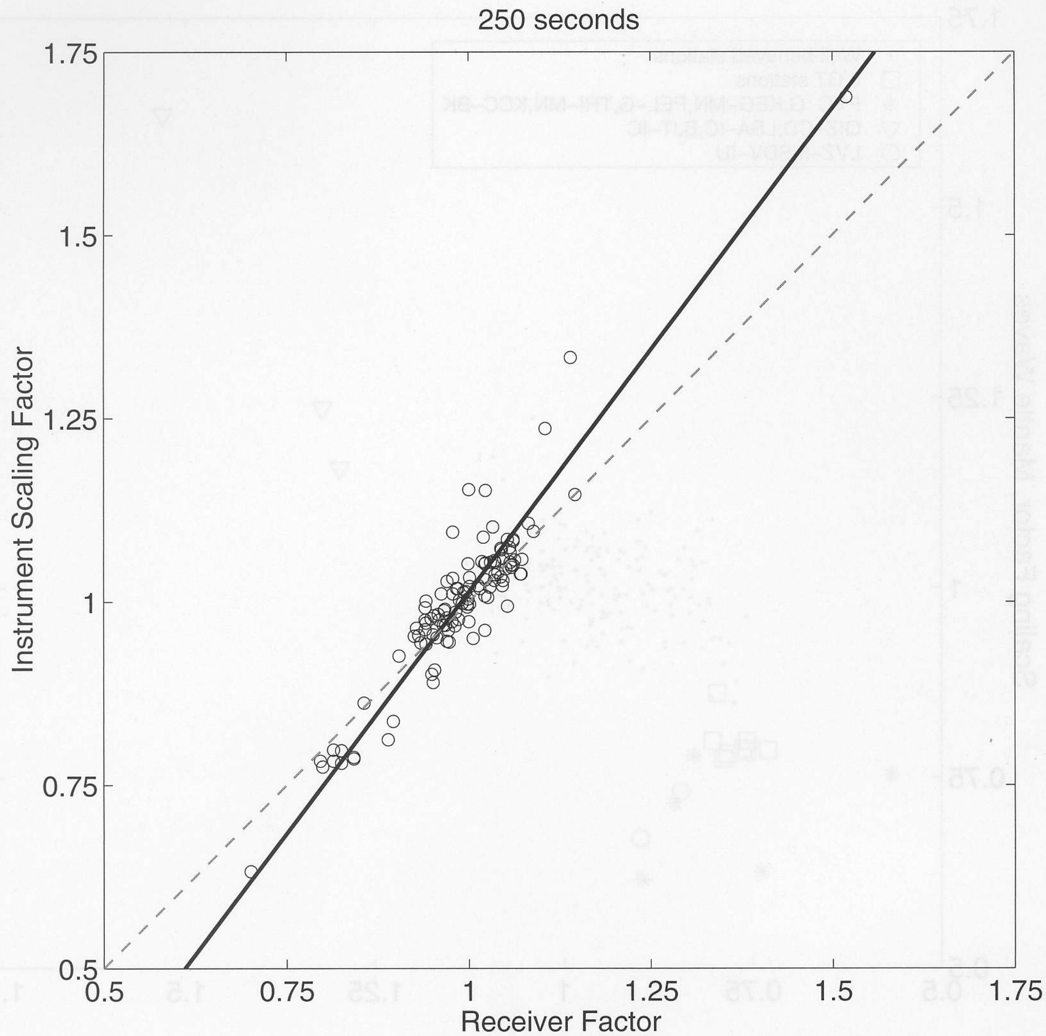

▲ **Figure 10.** Station-by-station comparison of the mantle-wave instrument scaling factors obtained in this study with receiver correction factors determined independently in a tomographic inversion of 250-s Rayleigh wave amplitudes (Dalton and Ekström, 2005). The vertical-component annual median scaling factors at each station have been averaged over the time period 1993–2002, with values smaller than 0.5 and larger than 2.0 excluded to maximize overlap with the data set of the tomographic inversion. Only those channels for which at least five years of annual median scaling factors are available have been plotted. The correlation coefficient for two sets of gain factors, compared here for 111 stations, is 0.93. Black line shows best fit through the data points; gray dashed line has a slope of 1.0.

REFERENCES

Butler, R., T. Lay, K. Creager, P. Earl, K. Fischer, J. Gaherty, G. Laske, B. Leith, J. Park, M. Ritzwoller, J. Tromp, and L. Wen (2004). The Global Seismographic Network surpasses its design goal, *Eos, Transactions of the American Geophysical Union* **85**, 225–229.

Dalton, C. A. and G. Ekström (2004). Upper-mantle attenuation structure as revealed by surface-wave amplitudes. *Eos, Transactions of the American Geophysical Union* **85** supplement F1416.

Dalton, C. A. and G. Ekström (2005). Global models of surface-wave attenuation, *Journal of Geophysical Research* (submitted).

Dziewonski, A. M. and D. L. Anderson (1981). Preliminary reference Earth model, *Physics of the Earth and Planetary Interiors* **257**, 297–381.

Dziewonski, A. M., T.-A. Chou, and J. H. Woodhouse (1981). Determination of earthquake source parameters from waveform data for studies of global and regional seismicity, *Journal of Geophysical Research* **86**, 2,825–2,853.

Ekström, G. and M. Nettles (1997). Calibration of the HGLP seismograph network and centroid-moment tensor analysis of significant earthquakes of 1976, *Physics of the Earth and Planetary Interiors* **101**, 219–243.

Ekström, G., A. M. Dziewoński, N. N. Maternovskaya, and M. Nettles (2005). Global seismicity of 2003: Centroid-moment tensor solutions for 1087 earthquakes, *Physics of the Earth and Planetary Interiors* **148**, 327–351.

Wielandt, E. and J. M. Steim (1986). A digital very-broad-band seismograph, *Annales Geophysicae* **4**, 227–232.

Woodward, R. L. and G. Masters (1989). Calibration and data quality of the long-period SRO/ASRO networks, 1977 to 1980, *Bulletin of the Seismological Society of America* **79**, 1,972–1,983.

Harvard University
Dept. of Earth and Planetary Sciences
20 Oxford Street
Cambridge, MA 02138
ekstrom@seismology.harvard.edu